SILICON SURFACE PASSIVATION BY ULTRATHIN Al_2O_3 FILMS AND Al_2O_3/SiN_x STACKS

Jan Schmidt, Boris Veith, Florian Werner, Dimitri Zielke, and Rolf Brendel
Institute for Solar Energy Research Hamelin (ISFH), Am Ohrberg 1, 31860 Emmerthal, Germany

ABSTRACT

We show that aluminum oxide (Al_2O_3) layers deposited by thermal as well as by plasma-assisted atomic layer deposition (ALD) are very well suited for the effective surface passivation of *p*-type silicon wafers. Surface recombination velocities (SRVs) well below 10 cm/s are measured for both ALD variants. The SRV strongly increases with decreasing film thickness if the Al_2O_3 films are <10 nm for thermal ALD and <5 nm for plasma ALD. Firing at 830°C in a conveyor-belt furnace deteriorates the passivation quality, in particular for ultrathin Al_2O_3 films. For Al_2O_3 films ≤10 nm the thermal stability of the Al_2O_3 was significantly improved by depositing a 75-nm capping layer of PECVD-SiN_x onto the Al_2O_3. Application of Al_2O_3 to the rear of PERC solar cells shows that high V_{oc} values above 660 mV and J_{sc} values of 40 mA/cm^2 are achievable, irrespective of the ALD variant applied. However, generally slightly higher efficiencies are obtained for Al_2O_3 deposited by plasma ALD. The plasma ALD layers result in the highest efficiency of 21.1%.

INTRODUCTION

In recent years, aluminum oxide (Al_2O_3) grown by atomic layer deposition (ALD) has been identified as a dielectric material very well suited for the surface passivation of lowly doped *p*- and *n*-type silicon wafers [1-4] as well as highly doped p^+ silicon surfaces [5,6]. There are fundamental advantages over other dielectric materials (such as SiN_x or SiO_x) frequently used for the surface passivation of silicon solar cells. Importantly, as Al_2O_3 is a negative-charge dielectric, no parasitic shunting [7] occurs when applied to the rear of passivated emitter and rear cells (PERC) on *p*-type silicon. This has recently led to cell efficiencies exceeding 20% [8] for simplified PERC solar cells on *p*-type silicon and to efficiencies >23% [9] on *n*-type silicon wafers with Al_2O_3-passivated p^+ front emitter. Also, we have recently demonstrated that ALD-Al_2O_3 is well compatible with standard firing steps used for the fabrication of metal contacts in screen-printed solar cells. Hence, Al_2O_3 could be an important component for future industrial high-efficiency solar cells.

In contrast to deposition techniques conventionally applied in photovoltaics, such as plasma-enhanced chemical vapor deposition (PECVD), ALD consists of two self-limiting half-reactions, which implies numerous advantages: (i) ALD results in highly conformal coatings, which allows to passivate e.g. macropores or other complex surface structures, (ii) a generally pin-hole-free deposition is achieved, and (iii) as ALD is a self-limiting process extremely uniform films can be deposited over very large areas. The main disadvantage of ALD for photovoltaic applications is its relatively low deposition rate. This disadvantage could be overcome by depositing ultrathin ALD-Al_2O_3 films and capping them with a thicker film of e.g. PECVD-SiN_x or SiO_x or by the development of advanced fast ALD processes.

In this contribution, we study the dependence of the surface passivation quality on the Al_2O_3 film thickness for films deposited by two different ALD techniques, namely thermal ALD and plasma-assisted ALD. We examine the effect of a PECVD-SiN_x capping layer on top of the Al_2O_3 film on the firing stability of the surface passivation quality and finally present our latest PERC cell results.

THERMAL AND PLASMA-ASSISTED ALD

In the ALD process, one monolayer of Al_2O_3 is grown per cycle. Each cycle consists of two half-reactions, as depicted in Fig. 1. In the first half-reaction, trimethylaluminum (TMA) molecules react with hydroxyl (OH) groups attached to the surface. At the end of the first half-reaction, Al atoms and methyl groups cover the surface and the remaining TMA molecules in the deposition chamber are no longer able to react with the surface. After purging the deposition chamber with nitrogen or oxygen gas, the second half-reaction of the ALD cycle starts. We apply two different realization forms for the second half-reaction: in the *thermal ALD* process, water vapor is injected into the deposition chamber. The H_2O molecules react very fast with the Al-CH_3 complex attached to the surface. Hydrogen reacts with the methyl group to methane and oxygen reacts with aluminum to aluminum oxide. In the *plasma-assisted ALD* process, an oxygen plasma is ignited above the substrate, generating oxygen radicals which effectively react with the methyl groups and the aluminium at the surface. In the FlexAL deposition system from Oxford Instruments applied in this study an inductively coupled plasma (ICP) source is used, which means that the oxygen plasma is not in direct contact with the silicon wafer during Al_2O_3 deposition. This type of remote-plasma deposition technique is known to create almost no plasma damage at the surface, and is hence well suited for an excellent silicon surface passivation. In our FlexAL system, thermal as well as plasma-assisted ALD of Al_2O_3 can be performed in the same deposition chamber. Hence, the FlexAL is well suited for a direct comparison of both ALD techniques.

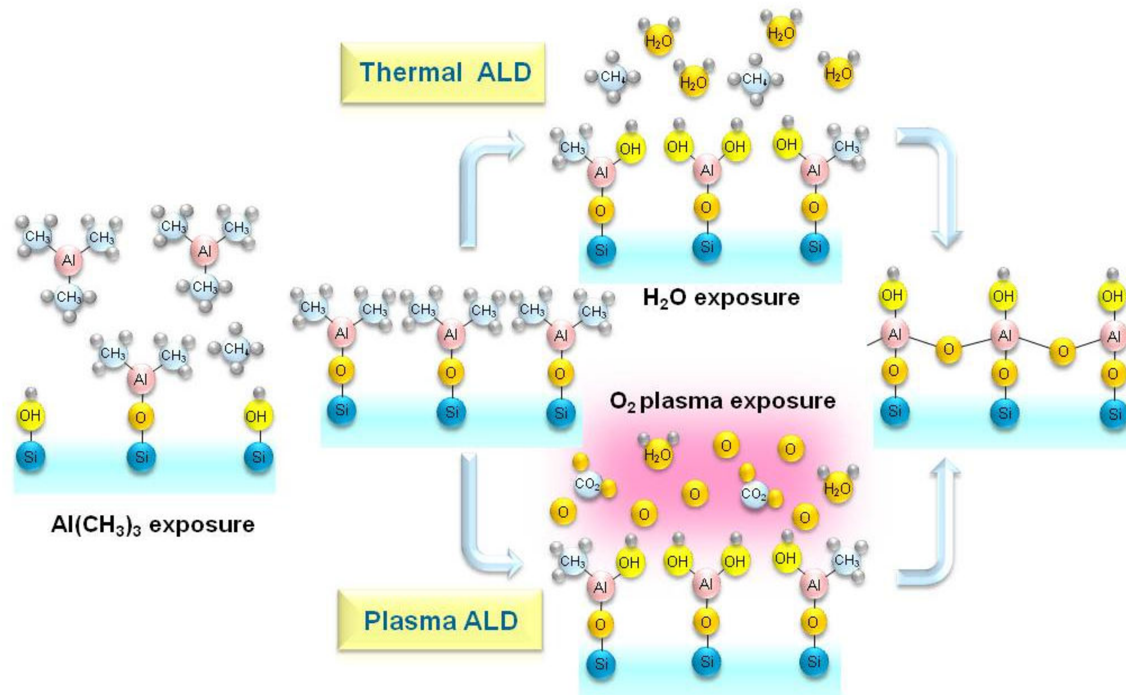

Fig.1. Schematic of one cycle of a thermal and a plasma-assisted atomic layer deposition (ALD) process. Each cycle consists of two half-steps: first, the trimethylaluminum (TMA) molecules attach to the hydroxyl groups attached to the silicon surface; second, the molecules are oxidized by H_2O (thermal ALD) or an O_2 plasma (plasma ALD).

Figure 2 shows the Al_2O_3 thickness, measured using an in-situ ellipsometer (Woollam M-2000F) integrated into our ALD system, as a function of the number of cycles. Figure 2 compares the growth per cycle (GPC) for plasma ALD and thermal ALD at a fixed deposition temperature of 200°C. Typical cycle durations are in the range 4 – 6 s. As can be seen from Fig. 2, plasma ALD results in a 60% higher GPC than thermal ALD at 200°C. However, the deposition rates obtained for both techniques are below 2 nm/min which means that for photovoltaic applications, where high throughput is required, only ultrathin Al_2O_3 layers are conceivable. This makes stacks of ALD-Al_2O_3 and SiN_x or SiO_x (deposited e.g. by PECVD) a very interesting option for industrial solar cells. Most recently is has been shown that by spatial separation of the half-reactions very high deposition rates up to 1 nm/s are achievable using ALD [10]. These recent developments could make ALD a near-term option for the surface passivation of next-generation industrial solar cells.

Figure 3 shows a spatially resolved ellipsometry measurement of the thickness distribution of an Al_2O_3 layer deposited in our FlexAL system on a polished 6” silicon wafer. The Al_2O_3 film was deposited at 200°C using 500 cycles of plasma-assisted ALD. The thickness homogeneity over the entire wafer is 0.4%. We also measure an excellent thickness homogeneity better than 0.5% on 6” wafers using thermal ALD.

Figure 4 shows a dynamic infrared lifetime mapping (*dynamic ILM*) [11] measurement of the effective carrier lifetime τ_{eff} of a 1-Ωcm *p*-type float-zone silicon wafer.

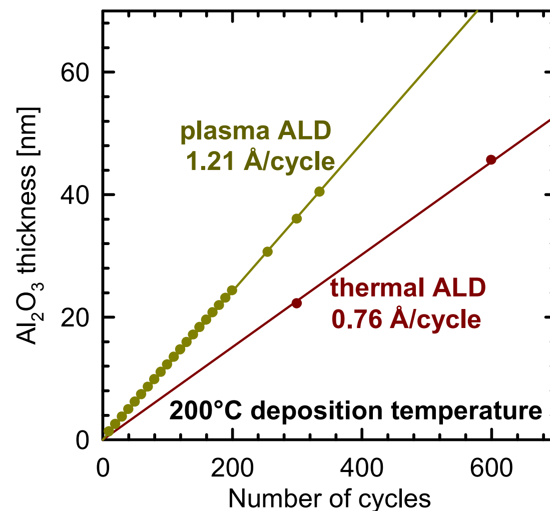

Fig. 2. Al_2O_3 thickness as a function of the number of cycles for (i) plasma-assisted ALD and (ii) thermal ALD. The film thickness was determined by in-situ ellipsometry and the growth per cycle (GPC) was determined from the linear fits to the measured data.

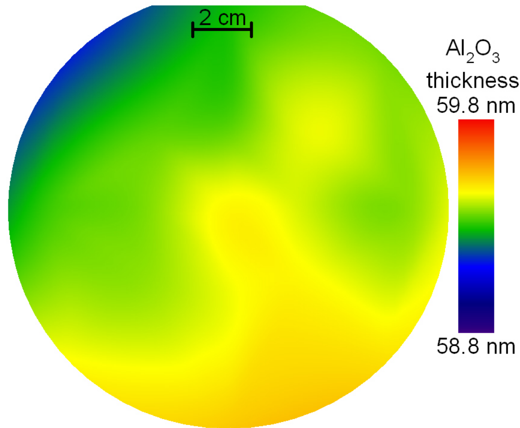

Fig. 3. Thickness of an Al_2O_3 layer deposited on a polished 6” silicon wafer measured using ellipsometry. The Al_2O_3 film was deposited at 200°C using 500 cycles of plasma-assisted ALD. The thickness homogeneity over the entire wafer is 0.4%.

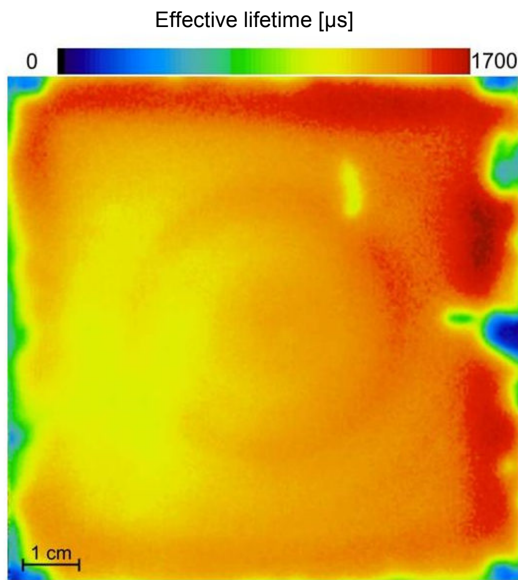

Fig. 4. Spatially resolved measurement of the effective lifetime τ_{eff} on a 1-Ωcm *p*-type float-zone silicon wafer using the dynamic infrared lifetime mapping (*dynamic ILM*) [11] technique. Both wafer surfaces are passivated by 20 nm of Al_2O_3 deposited using plasma-assisted ALD at 200°C. After deposition the sample was annealed at 425°C to improve the passivation quality. The area-averaged lifetime is 1.3 ms and the standard deviation is 0.2 ms.

Both wafer surfaces are passivated by 20 nm of Al_2O_3 deposited using plasma-assisted ALD at 200°C. After deposition the sample was annealed at 425°C to improve the passivation quality. The area-averaged lifetime is 1.3 ms and the standard deviation is 0.2 ms, demonstrating that a very good homogeneity of the passivation quality is achieved using ALD.

PLASMA VS THERMAL ALD

In order to evaluate the surface passivation quality of Al_2O_3 deposited by plasma ALD versus thermal ALD, we perform photoconductance decay measurements using a Sinton lifetime tester. We use 290 µm thick (100)-oriented low-resistivity (1.5 Ωcm) *p*-type float-zone silicon (FZ-Si) wafers coated with Al_2O_3 films on both wafer surfaces at deposition temperatures ranging from 200 to 260°C. To convert the measured effective lifetime values τ_{eff} into effective surface recombination velocities (SRVs) S_{eff}, we use the intrinsic bulk lifetime of silicon according to the parameterization published in Ref. 12. If not stated otherwise, in this study we report lifetimes measured at an injection density of $\Delta n = 10^{15}$ cm^{-3}. For the used 1.5 Ωcm FZ-Si wafers, the corresponding bulk lifetime amounts to τ_b = 3.4 ms. Prior to surface passivation all wafers were damage-etched and RCA-cleaned. Figure 5 shows the measured effective lifetime τ_{eff} as a function of the Al_2O_3 layer thickness in the as-deposited state (i.e. without any post-annealing). Effective lifetimes in the range 3 – 5 µs (circles in Fig. 5), corresponding to an effective surface recombination velocity (SRV) S_{eff} of ~10^4 cm/s, show that Al_2O_3 deposited by plasma ALD provides virtually *no surface passivation in the as-deposited state*. Conversely, Al_2O_3 layers deposited by thermal ALD provide a *good level of surface passivation already in the as-deposited state* (triangles in Fig. 5) if they are sufficiently thick. For the thermal ALD an increasing effective lifetime with increasing Al_2O_3 thickness is observed. As can be seen from Fig. 5, for a 10 nm thick Al_2O_3 film deposited by thermal ALD an effective lifetime of only 24 µs is measured, corresponding to an S_{eff} of 670 cm/s, whereas for a 30 nm thick layer a τ_{eff} of already 290 µs is obtained.

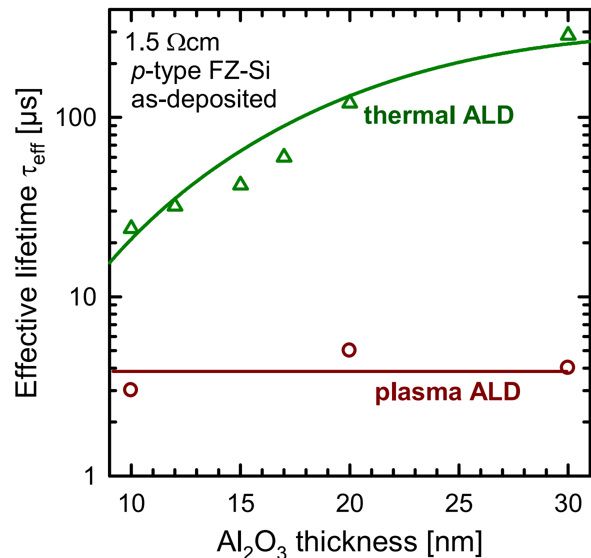

Fig. 5. Measured effective lifetime τ_{eff} as a function of the Al_2O_3 layer thickness in the as-deposited state (i.e. without any post-annealing). The lines are guides to the eyes.

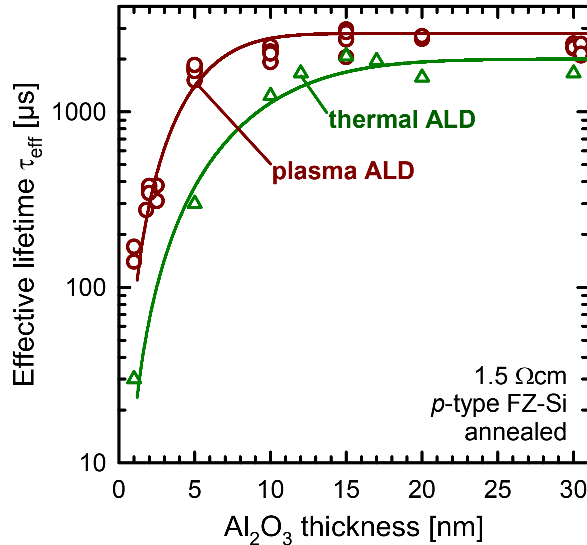

Fig. 6. Measured effective lifetime τ_{eff} as a function of the Al_2O_3 layer thickness after post annealing for 15 min at 425°C for the plasma ALD samples and at 350°C for the thermal ALD samples. The lines are guides to the eyes.

The latter lifetime corresponds to an effective SRV of S_{eff} = 45 cm/s. We conclude that using thermal ALD it is in fact possible to realize a relatively good surface passivation quality in the as-deposited state applying processing temperatures ≤260°C. No satisfactory surface passivation quality is however achieved for very thin layers (<20 nm). Similar results have recently been reported for *n*-type silicon wafers [4]. The completely different passivation properties of Al_2O_3 deposited by plasma and by thermal ALD could suggest that the growth mechanisms are different in both cases. Another potentially important difference between thermal and plasma ALD recently pointed out by Dingemans et al. [4] is that during plasma ALD the interface is exposed to very hard UV radiation emitted by the O_2 plasma, which might damage the interface. This damage could be annealed out during the post-annealing treatment.

Figure 6 shows the dependence of τ_{eff} on the Al_2O_3 thickness after a post annealing treatment of the samples. We have optimized the post annealing treatment and found that relatively broad temperature windows of approximately ±50°C can be applied to achieve an excellent surface passivation. The samples shown in Fig. 6 were annealed for 15 min at 425°C for the plasma ALD samples and at 350°C for the thermal ALD samples. By comparing Figs. 5 and 6 it can be seen that a dramatic increase in τ_{eff} is observed after post annealing. The Al_2O_3 deposited by plasma ALD shows, independent of the layer thickness, higher τ_{eff} values than the samples passivated by thermal ALD, which means that the post annealing reverses the trend measured in the as-deposited state (Fig. 5). For the plasma ALD films, maximum lifetimes of 3 ms are measured for an Al_2O_3 thickness above 10 nm, which corresponds to an ultralow effective SRV of S_{eff} = 0.6 cm/s using the intrinsic bulk lifetime parameterization of Kerr and Cuevas [12]. For the thermal ALD films, slightly lower maximum lifetimes of 2 ms are measured, still leading to an outstanding S_{eff} of 3 cm/s. The differences between thermal and plasma ALD become more pronounced for ultrathin (< 10 nm) layers. While the plasma ALD layer shows only a small deterioration until a film thickness of 5 nm is reached, the thermal ALD Al_2O_3 layer shows a pronounced deterioration in its passivation quality already for film thicknesses below 10 nm. For an extremely thin Al_2O_3 layer of only 1 nm thickness, we still measure a τ_{eff} of 170 µs (S_{eff} = 80 cm/s) for the plasma ALD sample, but only τ_{eff} = 30 µs (S_{eff} = 520 cm/s) for the thermal ALD sample. Our results show that the surface passivation quality of ultrathin Al_2O_3 films deposited by plasma ALD is clearly superior to that of films deposited by thermal ALD. To find out the reason for the increasing S_{eff} with decreasing Al_2O_3 thickness, we have measured some of our samples using the lifetime-corona technique [13]. Our experimental results show that the very large negative fixed charge density Q_f within our Al_2O_3 films, which is in the range of $Q_f = -4\text{-}6\times10^{12}$ cm^{-3}, does not change with the Al_2O_3 thickness, however, the interface state density strongly increases with decreasing film thickness for the ultrathin layers [14]. This suggests that the defect states responsible for the fixed charges are located extremely close (< 1 nm) to the interface. The main reason for the strong increase in S_{eff} with decreasing Al_2O_3 thickness is however unambiguously an increase of the interface state density.

FIRING STABILITY

We exposed 1.5 Ωcm *p*-type FZ-Si wafers passivated with (i) single layers of plasma ALD-Al_2O_3 and (ii) stacks of plasma ALD-Al_2O_3 and PECVD-SiN_x (75 nm thick) to a firing treatment typically applied in standard screen-printing solar cell production processes.

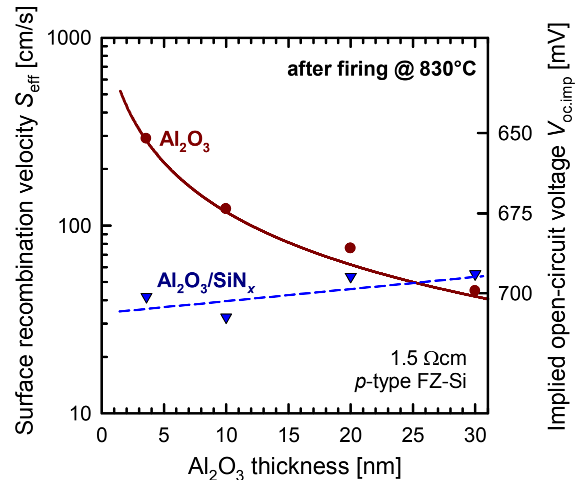

Fig. 7. Effective SRV S_{eff} measured at an injection density of 10^{15} cm^{-3} after firing at 830°C as a function of Al_2O_3 layer thickness for (i) a single layer of plasma ALD-Al_2O_3 and (ii) stacks of Al_2O_3 and PECVD-SiN_x (75 nm thick). The right scale shows the implied open-circuit voltage corresponding to the measured S_{eff}.

Table 1: One-sun parameters measured under standard testing conditions of the best PERC silicon solar cells with 3 different rear surface passivations: (i) thermal SiO_2 (220 nm), (ii) thermal ALD Al_2O_3 (30 nm)/PECVD-SiN_x (100 nm) stacks, and (iii) Al_2O_3(30 nm)/PECVD-SiO_x (200 nm) stacks. All cells were fabricated on 0.5-Ωcm FZ *p*-Si wafers. The aperture cell area is 4 cm^2.

Rear side passivation	**V_{oc} [mV]**	**J_{sc} [mA/cm^2]**	***FF* [%]**	**η [%]**
Thermal SiO_2	657	39.1	78.9	20.2
Thermal ALD Al_2O_3/SiN_x	660	39.4	78.4	20.4
Plasma ALD Al_2O_3/SiO_x	666	40.1	79.0	21.1

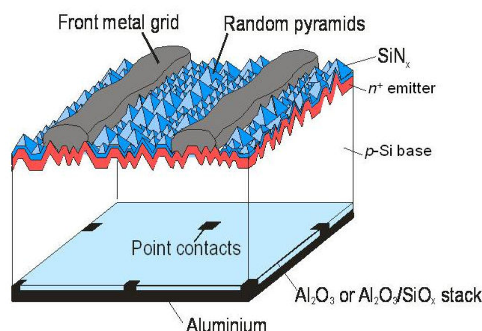

Fig. 8. PERC-type solar cell structure used to demonstrate the applicability of different rear surface passivation schemes.

Firing experiments were performed in an industrial infrared conveyor-belt furnace (Centrotherm Contact Firing Furnace DO 8.600-300-FF) at a peak temperature of ~830°C for ~3 s. The peak temperature stated is the actual temperature measured during firing using a data logger. The set temperature was 860°C. Figure 7 shows the effective SRV S_{eff} measured at an injection density of 10^{15} cm^{-3} after firing as a function of Al_2O_3 layer thickness. The right scale in Fig. 7 shows the implied open-circuit voltage corresponding to the measured SRV. Compared to the S_{eff} values measured before firing, which are always well below 10 cm/s (see above), we measure a pronounced increase in S_{eff} due to the firing. For an Al_2O_3 thickness ≥20 nm we measure S_{eff} values in the vicinity of 50 cm/s after firing, which holds for single layers of Al_2O_3 (red circles in Fig. 7) as well as for Al_2O_3/SiN_x stacks (blue triangles in Fig. 7). For Al_2O_3 films ≤10 nm the thermal stability of the Al_2O_3 is significantly improved by depositing a 75-nm capping layer of SiN_x onto the Al_2O_3, which is probably due to the very high (10-15 at.%) hydrogen content in the PECVD-SiN_x film. Deposition of SiN_x onto the 3.6-nm Al_2O_3 layer alone increases the lifetime from 550 to 700 µs (before firing) [3], which is most likely due to hydrogen diffusing from the SiN_x through the ultrathin Al_2O_3 to the interface, where it effectively passivates dangling bonds. For ultrathin Al_2O_3 layers (≤10 nm covered by 75 nm SiN_x we measure S_{eff} values in the range between 30 and 40 cm/s. The surface passivation quality of these stacks after firing is hence compatible with an open-circuit voltage V_{oc} exceeding 700 mV, which is well acceptable for future industrial high-efficiency solar cells.

PERC SOLAR CELLS

In order to verify the suitability of the different dielectric layers to the rear surface passivation of *p*-type silicon solar cells, we have fabricated passivated emitter and rear cells (PERC) using the process sequence described in Ref. 8. Figure 8 shows the cell structure featuring a PECVD-SiN_x-passivated 100 Ω/sq phosphorus-diffused n^+ front emitter and a rear surface passivated by the dielectric layer systems shown in the first column of Table 1. The front grid is made by shadow-mask evaporation of aluminum and the rear is fully metalized by full-area aluminum evaporation (4% rear metallization fraction) after point contact openings have been generated. As a reference process we use an SiO_2 rear passivation grown by wet thermal oxidation at 1000°C [8]. Table 1 summarizes the one-sun parameters of the best PERC solar cells, as measured under standard testing conditions (25°C, 100 mW/cm^2, AM 1.5 G). Remarkably, the measured open-circuit voltages V_{oc} and short-circuit current densities J_{sc} of the Al_2O_3-passivated cells are higher than the V_{oc} and J_{sc} values of the SiO_2-passivated reference cell. V_{oc} values of Al_2O_3-passivated cells are all ≥660 mV and J_{sc} values are in the vicinity of 40 mA/cm^2, demonstrating that parasitic shunting effects are absent in these cells. On top of the very thin Al_2O_3 layers we have deposited thicker PECVD SiO_x or SiN_x layers to improve the internal rear reflection of the cell. Importantly, there is **no significant difference between thermal and plasma ALD**. However, slightly higher open-circuit voltages are typically obtained for Al_2O_3 films deposited by plasma ALD, in agreement with the slightly better passivation measured on lifetime test structures. The results compiled in Table 1 clearly demonstrate that plasma and thermal ALD are both well suited for the fabrication of high-efficiency PERC cells with efficiencies exceeding 20%. The highest efficiency of **21.1%** in Table 1 is achieved for the plasma ALD Al_2O_3 layer, whereas the thermal ALD results in a maximum efficiency of 20.4%, which is comparable to the thermal oxide reference.

CONCLUSIONS

We have demonstrated that Al_2O_3 layers deposited by plasma-assisted as well as by thermal ALD are very well suited for the surface passivation of *p*-type silicon wafers. In the case of **plasma ALD**, however, the as-deposited films show virtually no surface passivation, whereas after post-annealing treatment **surface recombination velocities below 1 cm/s were measured**. For thermal ALD, a satisfactory level of surface passivation was already measured in the as-grown state, which improved with increasing film thickness. For a 30 nm thick as-grown thermal ALD Al_2O_3 layer a SRV of 45 cm/s was measured. After post annealing this SRV decreased to **only 3 cm/s**, making **thermal ALD** also an excellent choice for the surface passivation of silicon solar cells. In general, the passivation quality was found to deteriorate with decreasing Al_2O_3 film thickness. However, for plasma ALD Al_2O_3 films a pronounced deterioration of the SRV was only observed for layer thicknesses < 5 nm, whereas thermal ALD films already deteriorated in the surface passivation level below 10 nm.

Firing at 830°C in a conveyor-belt furnace was found to degrade the passivation quality, in particular for ultrathin Al_2O_3 films. **For Al_2O_3 films ≤10 nm the thermal stability of the Al_2O_3 was significantly improved by depositing a 75-nm capping layer of SiN_x** onto the Al_2O_3, which is probably due to the very high hydrogen content in the PECVD-SiN_x film. For ultrathin Al_2O_3 layers we measured SRVs between 30 and 40 cm/s after firing, which is compatible with implied V_{oc} values exceeding 700 mV.

Al_2O_3 films deposited by thermal and by plasma ALD were applied as rear passivation layers to PERC solar cells and **no significant difference between thermal and plasma ALD** was observed. V_{oc} values in the range 660 – 670 mV, J_{sc} values of ~40 mA/cm^2 and efficiencies exceeding 20% clearly indicate that parasitic shunting effects are absent in Al_2O_3-passivated cells. In average over many cells, slightly better cell results were obtained with plasma ALD. The maximum efficiency of 21.1% was achieved for a PERC cell with plasma ALD-Al_2O_3/ PECVD-SiO_x rear surface passivation.

Acknowledgments
Funding was provided by the State of Lower Saxony and the German Ministry for the Environment, Nature Conservation and Nuclear Safety (BMU) under contract number 0325050 (“ALD”).

REFERENCES

[1] G. Agostinelli, A. Delabie, P. Vitanov, Z. Alexieva, H.F.W. Dekkers, S. De Wolf, G. Beaucarne, *Sol. En. Mat. Sol. Cells* **90**, 3438 (2006).

[2] B. Hoex, S.B.S. Heil, E. Langereis, M.C.M. van de Sanden, W.M.M. Kessels, *Appl. Phys. Lett.* **89**, 042112 (2006).

[3] J. Schmidt, B. Veith, R. Brendel, *Phys. Status Solidi RRL* **3**, 287 (2009).

[4] G. Dingemans, R. Seguin, P. Engelhart, M.C.M. van de Sanden, W.M.M. Kessels, *Phys. Status Solidi RRL* **4**, 10 (2010).

[5] B. Hoex, J. Schmidt, R. Bock, P.P. Altermatt, M.C.M. van de Sanden, W.M.M. Kessels, Appl. Phys. Lett. **91**, 112107 (2007).

[6] J. Benick, A. Richter, M. Hermle, S.W. Glunz, *Physica Status Solidi RRL* **3**, 233 (2009)

[7] S. Dauwe, L. Mittelstädt, A. Metz, R. Hezel, *Progress in Photovoltaics* **10**, 271 (2002).

[8] J. Schmidt, A. Merkle, R. Brendel, B. Hoex, M.C.M. van de Sanden, W.M.M. Kessels, *Progress in Photovoltaics* **16**, 461 (2008).

[9] J. Benick, B. Hoex, M.C.M. van de Sanden, W.M.M. Kessels, O. Schultz, S.W. Glunz, *Appl. Phys. Lett.* **92**, 253504 (2008).

[10] www.tno.nl

[11] K. Ramspeck, S. Reissenweber, J. Schmidt, K. Bothe, R. Brendel, *Appl. Phys. Lett.* **93**, 102104 (2008).

[12] M.J. Kerr and A. Cuevas, *J. Appl. Phys.* **91**, 2473 (2002).

[13] S. Dauwe, J. Schmidt, A. Metz, R. Hezel, *Proc. 29th IEEE Photovolt. Spec. Conf.*, New Orleans, USA (IEEE, New York, 2002), p. 162.

[14] F. Werner, B. Veith, D. Zielke, L. Kühnemund, C. Tegenkamp, J. Schmidt, R. Brendel, *25th European Photovoltaic Solar Energy Conf.*, Valencia, Spain (2010).